Int J Adv Manuf Technol (2017) 89:2087–2098
DOI 10.1007/s00170-016-9213-0

ORIGINAL ARTICLE

Modeling of weld bead geometry on HSLA steel using response surface methodology

Mirza Jahanzaib[1] · **Salman Hussain**[1] · **Ahmad Wasim**[1] · **Haris Aziz**[1] · **Adnan Mirza**[1] · **Saif Ullah**[2]

Received: 4 March 2016 / Accepted: 25 July 2016 / Published online: 7 August 2016

Abstract With increasing requirements of higher strength to low weight ratio materials, high-strength low-alloy (HSLA) steel has achieved higher commercial importance. Plasma arc welding has the capability to join metals without edge preparation, weldment in a single pass and minimum angular distortion. Due to these embedded capabilities, plasma arc welding is preferred over conventional joining processes for HSLA steel applications involving part thickness greater than 3 mm. The quality of plasma arc-welded joints is highly dependent on input process parameters. This paper aims to develop empirical models for the prediction of weld bead geometry including front bead height, back bead height, front bead width, and back bead width. A series of tests were conducted to investigate the effect of four input process parameters including current, voltage, welding speed, and plasma gas flow rate on weld bead geometry using a face-centered central composite design. The confirmation experiments and ANOVA results validated the models within 95 % accuracy. Current was found to be the most influential factor affecting the weld bead geometry followed by speed. Furthermore, current and speed and speed and gas flow rates were identified as most influencing interaction factors. The innovation in this research is the empirical modeling of weld bead geometry for HSLA using plasma arc welding.

✉ Ahmad Wasim
wasim.ahmad@uettaxila.edu.pk

[1] Department of Industrial Engineering, University of Engineering and Technology, Taxila, Taxila, Pakistan

[2] School of Mechanical Science and Engineering, Huazhong University of Science and Technology, Wuhan, China

Keywords Weld bead geometry · Central composite design CCD · Plasma arc welding

1 Introduction

High-strength low-alloy (HSLA) steel is 20–30 % lighter than carbon steel for the same volume. Therefore, HSLA steel is preferred over carbon steel for the applications requiring high strength to low weight ratio, better resistance to atmospheric corrosion, and better mechanical properties. Due to these embedded properties, HSLA steel is used for highly demanding applications including oil and gas pipelines, storage tanks, bridges, offshore structures, and power transmission towers [1]. Welding is the most frequently employed fabrication process for HSLA steel. Its welding is being successfully carried out by shielded metal arc welding (SMAW), gas metal arc welding (GMAW), and gas tungsten arc welding (GTAW). For critical applications such as pressure vessels and rockets which involve part thickness greater than 3.0 mm with class 1 weld joint and radiographic qualification requirements [2], plasma arc welding (PAW) is preferred due to the following reasons: (1) PAW has the capability of greater energy concentration, improved arc stability, elevated heat content, and higher welding speeds. As a result, PAW has greater penetration capabilities than SMAW, GMAW, and GTAW [3]; (2) these arc welding processes (SMAW, GMAW, GTAW) require weld joint preparation in the form of V-groove or U-groove. Although weld without joint preparation can be performed, multi-passes are mandatory to meet the above said requirements resulting in increased welding time and higher chances of defects; (3) in some cases, SMAW is employed as a cheaper alternative to qualify class 1 weld joint. It is usually employed manually with a higher width to depth ratio as compared to PAW, resulting in angular distortion [4]; (4) filler

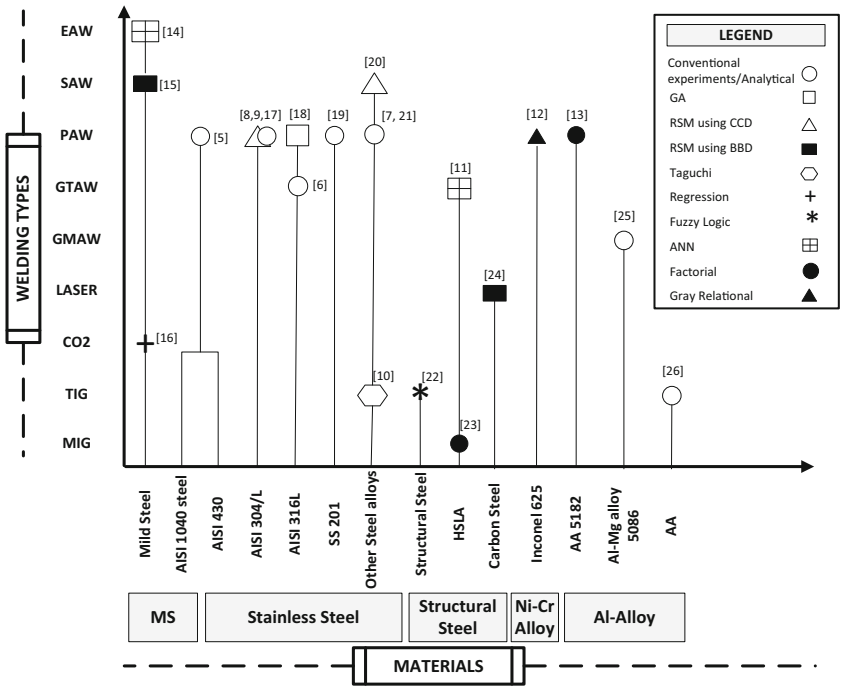

Fig. 1 Overview of research on welding types, alternative materials, and methods

metal is not required for PAW, whereas SMAW and GTAW require filler metal for sheet thickness greater than 3 mm; and (5) removal of slag is mandatory for the SMAW process.

The welding strength is measured by mechanical properties of weld (tensile strength, fracture strength, hardness, bend strength, corrosion resistance, and impact toughness) [1, 5–7]. These properties are directly related to weld bead geometry [8–13]. Therefore, the quality of plasma arc-welded joints in this research has been measured through weld bead geometry which consists of front bead height (FBH), back bead height (BBH), front bead width (FBW), and back bead width (BBW). The inappropriate weld bead geometry (FBH, BBH, FBW, and BBW) results in weld failure. The importance of weld bead geometry increases considerably as the failure of component can cause serious loss of life and resources. The weld bead geometry depends on certain welding process parameters. An expert welding operator selects these parameters using hit and trial and past knowledge. Different combinations of welding parameters are tried which may result in suboptimal solution. These trials can be avoided by conducting a systematic research to identify the effects of process parameters on weld bead geometry.

In this research, a comprehensive literature review has been carried out to highlight the previous work related to weld bead geometry on different materials using alternative welding processes. Figure 1 represents alternative approaches employed by previous researchers on various materials using different welding processes [5–26]. The materials are shown on *x*-axis, whereas welding processes are presented on *y*-axis. For example, Al-Faruk et al. [14] used analytical neural network (ANN) to model the weld bead geometry of mild steel plates using electron arc welding (EAW).

It is evident from Fig. 1 that a number of researchers investigated the effects of process parameters of PAW on AISI 1040, AISI 430, AISI 304/L, AISI 316L, SS 201, stainless steel, Inconel 625, and AA5182 [5, 7–9, 12, 13, 17–19, 21]. Similarly, conventional experiments/analytical, response surface methodology (RSM) using central composite design (CCD), factorial design, and gray relational approaches have been used by previous researchers to model weld bead geometry of PAW. In all these modeling approaches, RSM is one of the most effective approaches for the investigation of significant process parameters and prediction of responses using optimal combinations of significant process parameters [27].

It can be concluded from a detailed literature review that little or no work has been reported on HSLA steel to predict weld bead geometry using the PAW process. There fore, this research aims to develop models to correlate the effects of input process parameters on response variables, i.e., FBH, BBH, FBW, and BBW. This will aid in process parameter optimization for weld bead geometry. RSM with face-centered CCD and ANOVA has been applied to plan experiments and investigate the effects of process para meters.

Table 1 Chemical composition of HSLA steel

%C	%Si	%Mn	%P	%S	%Cr	%Ni	%Mo	%V
0.32	1.5	0.81	0.01	0.001	1.02	0.25	0.5	0.12

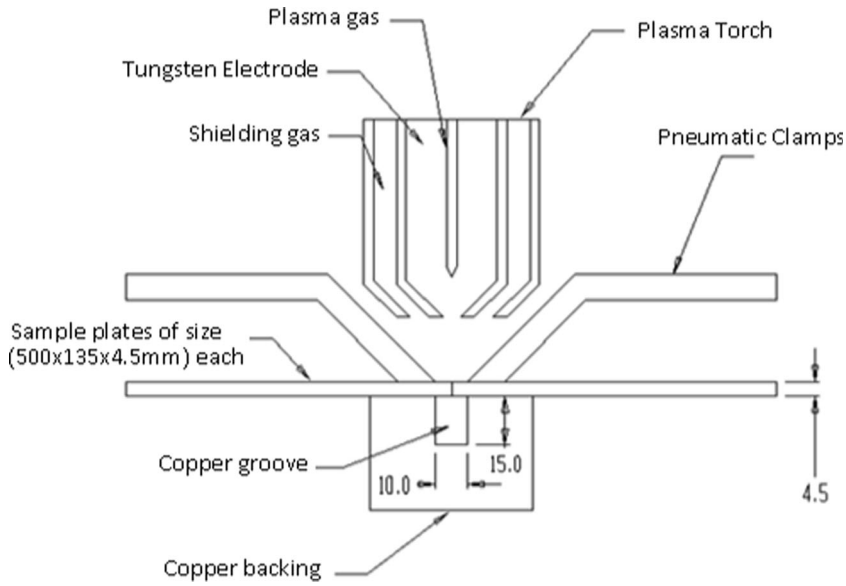

Fig. 2 Schematic showing orientation of sample, torch, clamping, and copper backing

2 Experimental procedure

This section describes the details regarding material composition, sample preparation, experimental setup, response measurements, and welding assumptions. PAW was performed on HSLA steel plates having chemical composition as shown in Table 1. The chemical composition of plates was verified through an XRF analyzer and wet analysis technique prior to experimentation.

The samples were prepared having dimensions 500 × 135 × 4.5mm^3 by using a CNC milling machine to form a square butt joint. To constraint the relative motion of plates, the samples were tack-welded from the ends.

All the samples were welded in a single pass on an automatic linear PAW machine with a maximum current capacity of 300 A. Argon was used as plasma, shielding, and backing gas. Welding samples were pneumatically clamped and kept stationary while the carriage with a plasma welding torch was moved at defined speeds. Copper backing was provided as a heat sink. Since this research was related to key hole PAW, a groove under the joint was provided to allow the flow of plasma gas through the sample plates. Orientation of the welding torch was kept vertical to sample plates. A tungsten electrode of 3.2 mm in diameter was used while shielding gas flow rate and backing gas flow rate were kept constant at 30 and 20 l/min, respectively. The schematic of PAW has been shown in Fig. 2.

The process parameters selected for the experiments were current, voltage, welding speed, and plasma gas flow rate. These parameters have been identified after a detailed literature review. The design space (provided in Table 2) has been selected on the basis of literature review, and trial runs were performed in laboratory. The response variables included FBH, BBH, FBW, and BBW as shown in Fig. 3.

To reveal the weld bead geometry, the samples were prepared by using standard metallurgical polishing techniques and etched with 5 % nital. The responses were measured using an optical microscope. The average of the three readings on each sample was taken as a final response value.

3 Experimental design

RSM has been used for modeling and analysis of weld bead geometry. In this method, multiple responses are influenced by input parameters with an aim to optimize the responses [28]. Four welding process parameters

Table 2 Process parameters with their design space

Process parameter	Units	Level 1	Level 2	Level 3
Current	Ampere	165	180	195
Voltage	Volts	29	29.5	30
Speed	Centimeter/min	20	22.5	25
Gas flow rate	Liter/min	4.5	4.75	5

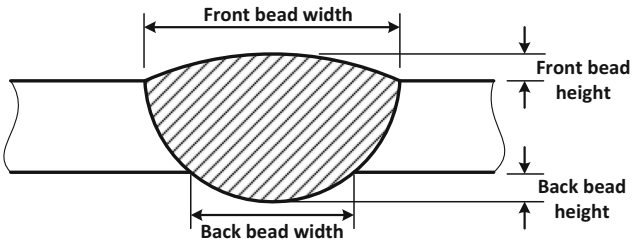

Fig. 3 Response variables of plasma arc weld

Table 3 Design matrix

Run	Input variables				Response variables			
	Current (A)	Voltage (V)	Speed (cm/min)	Gas flow rate (l/min)	Front bead height (mm)	Back bead height (mm)	Front bead width (mm)	Back bead width (mm)
1	180.00	29.50	22.50	4.75	0.19	0.69	5.83	2.50
2	180.00	29.50	22.50	4.50	0.12	0.58	6.23	2.80
3	195.00	30.00	25.00	5.00	0.08	0.75	6.228	3.23
4	180.00	29.50	22.50	4.75	0.18	0.64	5.63	2.59
5	165.00	29.00	25.00	5.00	0.44	0.42	4.42	2.69
6	180.00	29.00	22.50	4.75	0.20	0.67	6.195	2.81
7	165.00	29.00	20.00	4.50	0.36	0.20	5.71	2.654
8	165.00	30.00	25.00	4.50	0.40	0.22	4.33	2.246
9	180.00	29.50	20.00	4.75	0.12	0.70	6.34	3.22
10	165.00	30.00	20.00	5.00	0.37	0.39	5.47	2.51
11	195.00	29.00	25.00	4.50	0.05	0.90	6.25	2.75
12	165.00	30.00	20.00	4.50	0.38	0.27	5.80	2.90
13	180.00	29.50	22.50	5.00	0.19	0.67	6.31	2.85
14	165.00	29.00	25.00	4.50	0.34	0.37	4.323	2.70
15	180.00	30.00	22.50	4.75	0.14	0.75	6.13	2.79
16	180.00	29.50	22.50	4.75	0.17	0.69	5.73	2.50
17	165.00	29.00	20.00	5.00	0.35	0.49	5.75	2.90
18	180.00	29.50	25.00	4.75	0.11	0.71	5.6	2.56
19	195.00	29.00	20.00	5.00	0.04	0.75	7.23	4.20
20	195.00	29.00	25.00	5.00	0.08	0.69	6.21	3.37
21	195.00	29.00	20.00	4.50	0.09	0.65	7.45	4.23
22	195.00	29.50	22.50	4.75	0.06	0.77	6.3	3.74
23	195.00	30.00	25.00	4.50	0.02	1.00	6.33	2.78
24	180.00	29.50	22.50	4.75	0.15	0.63	5.82	2.70
25	180.00	29.50	22.50	4.75	0.18	0.65	5.64	2.66
26	180.00	29.50	22.50	4.75	0.19	0.62	5.79	2.60
27	195.00	30.00	20.00	5.00	0.01	0.89	7.16	4.42
28	195.00	30.00	20.00	4.50	0.02	0.78	7.10	4.31
29	165.00	30.00	25.00	5.00	0.50	0.20	4.263	2.43
30	165.00	29.50	22.50	4.75	0.33	0.42	4.68	2.40

(current (A), voltage (B), welding speed (C), and plasma gas flow rate (D)) have been used to investigate their effects on response variables, i.e., FBH, BBH, FBW, and BBW.

In RSM, when all the independent (input) variables (A, B, C, and D) are measurable, controllable and continuous with negligible error, the response surface Y can be expressed by the following relation (Eq. 1).

$$Y = f(A, B, C, D) \tag{1}$$

In practical applications of RSM, it is always compulsory to model the true response surface. The approximating model is an empirical model and is based on experimental observations from the process. The empirical model is either first order (Eq. 2) or second order (Eq. 3) and can be simplified as:

$$Y = \beta_0 + \sum_{i=1}^{n} \beta_i X_i + \tag{2}$$

$$Y = \beta_0 + \beta_1 X_1 + \beta_2 X^2 + \tag{3}$$

where β_0, β_i, β_1, and β_2 are approximating functions of parameters, x_i is input parameter, and y is response variable.

3.1 Central composite design

All the experiments performed in this research are based on a faced-centered composite design. In the faced-centered

Table 4 Reduced ANOVA table of front bead height, back bead height, front bead width, and back bead width

Front bead height						
Source	Some of square	DF	Mean square	F value	*P* value (prob > F)	
Model	0.55	7	0.079	89.34	<0.0001	Significant
A-current	0.51	1	0.51	574.14	<0.0001	
B-voltage	5.000E−005	1	5.000E−005	0.057	0.8141	
C-speed	4.356E−003	1	4.356E−003	4.94	0.0369	
D-gas flow rate	4.356E−003	1	4.356E−003	4.94	0.0369	
AB	5.256E−003	1	5.256E−003	5.96	0.0232	
CD	8.556E−003	1	8.556E−003	9.70	0.0051	
A^2	0.023	1	0.023	25.69	<0.0001	
Residual	0.019	22	8.825E−004			
Lack of fit	0.018	17	1.075E−003	4.74	0.0467	Significant
Pure error	1.133E−003	5	2.267E−004			
Cor total	0.57	29				
		Std. dev.	0.030	R^2	0.9660	
		Mean	0.20	Adj R^2	0.9552	
		C.V. %	15.21	Pred R^2	0.9402	
		PRESS	0.034	Adeq precision	29.279	
Back bead height						
Model	1.23	7	0.12	49.04	<0.0001	Significant
A-current	0.98	1	0.98	391.89	<0.0001	
B-voltage	6.722E−004	1	6.722E−004	0.27	0.6101	
C-speed	1.089E−003	1	1.089E−003	0.44	0.5173	
D-gas flow rate	4.356E−003	1	4.356E−003	1.74	0.2026	
AB	0.043	1	0.043	17.22	0.0005	
AC	0.011	1	0.011	4.20	0.0545	
AD	0.030	1	0.030	11.90	0.0027	
BC	0.013	1	0.013	5.06	0.0365	
CD	0.069	1	0.069	27.55	<0.0001	
A^2	0.075	1	0.075	30.09	<0.0001	
Residual	0.048	19	2.501E−003			
Lack of fit	0.043	14	3.070E−003	3.39	0.0925	Not significant
Pure error	4.533E−003	5	9.067E−004			
Cor total	1.27	29				
		Std. dev.	0.050	R^2	0.9627	
		Mean	0.61	Adj R^2	0.9431	
		C.V. %	8.26	Pred R^2	0.8821	
		PRESS	0.15	Adeq precision	24.677	
Front bead width						
Model	19.74	6	3.29	133.77	<0.0001	Significant
A-current	13.37	1	13.37	543.47	<0.0001	
C-speed	5.62	1	5.62	228.40	<0.0001	
D-gas flow rate	0.013	1	0.013	0.52	0.4761	
AC	0.14	1	0.14	5.51	0.0279	
A^2	0.52	1	0.52	21.00	0.0001	
D^2	0.53	1	0.53	21.61	0.0001	
Residual	0.57	23	0.025			
Lack of fit	0.53	18	0.029	3.73	0.0753	Not significant
Pure error	0.039	5	7.840E−003			
Cor total	20.31	29				
		Std. dev.	0.16	R^2	0.9721	

Table 4 (continued)

		Mean	5.87	Adj R^2	0.9649	
		C.V. %	2.67	Pred R^2	0.9593	
		PRESS	0.83	Adeq precision	38.206	
Back bead width						
Model	10.07	6	1.68	57.50	<0.0001	Significant
A-current	5.12	1	5.12	175.43	<0.0001	
C-speed	2.41	1	2.41	82.62	<0.0001	
D-gas flow rate	0.084	1	0.084	2.88	0.1032	
AC	1.07	1	1.07	36.56	<0.0001	
CD	0.11	1	0.11	3.66	0.0681	
A^2	1.28	1	1.28	43.86	<0.0001	
Residual	0.67	23	0.029			
Lack of fit	0.64	18	0.035	5.32	0.0366	Significant
Pure error	0.033	5	6.657E−003			
Cor total	10.74	29				
		Std. dev.	0.17	R^2	0.9375	
		Mean	2.97	Adj R^2	0.9212	
		C.V. %	5.76	Pred R^2	0.8815	
		PRESS	1.27	Adeq precision	23.778	

composite design, if the number of factors is represented by k and the number of center points by m, then the total number of experiments can be calculated by the following relation (Eq. 4) [28].

$$n = 2^k + 2k + m \tag{4}$$

Equation 4 is composed of factorial points (2^k), axial points ($2k$), and 4~6 center points (m). It can be established from Eq. 4 that for the current research involving four factors (A, B, C, and D), the design consists of 30 experiments (16 factorial points, 8 axial points, and 6 center points). In the face-centered composite design, axial points are used to detect the

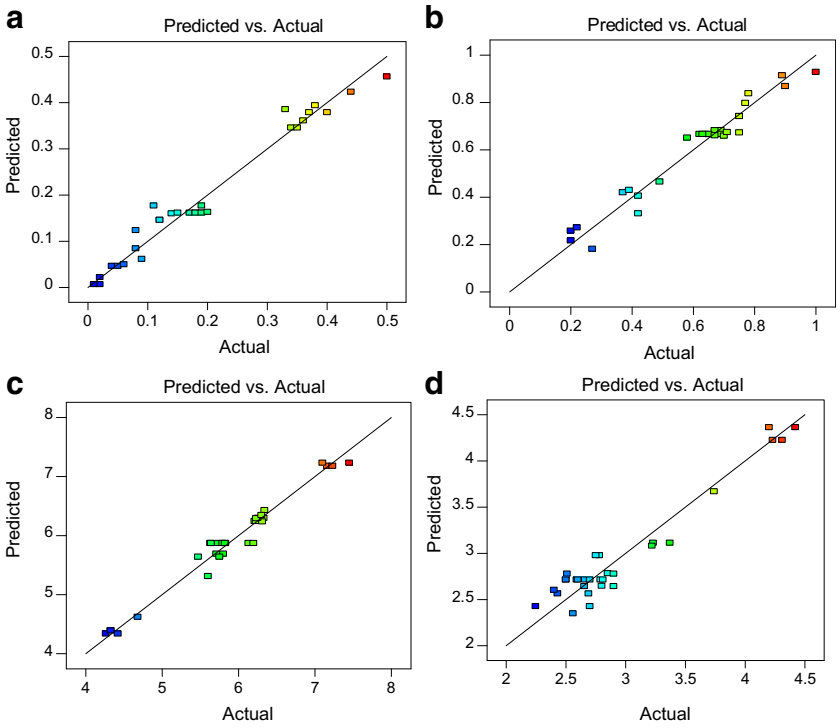

Fig. 4 **a** Predicted vs actual response for front bead height. **b** Predicted vs actual response for front bead width. **c** Predicted vs actual response for back bead height. **d** Predicted vs actual response for back bead width

Table 5 Comparison of predicted and actual response variables along with percentage error

Experiment no.	Process parameters				Predicted responses				Actual responses				Percentage error			
	Current	Voltage	Welding speed	Flow rate	Front bead height (mm)	Back bead height (mm)	Front bead width (mm)	Back bead width (mm)	Front bead height (mm)	Back bead height (mm)	Front bead width (mm)	Back bead width (mm)	Front bead height (mm)	Back bead height (mm)	Front bead width (mm)	Back bead width (mm)
1	172	29.2	21	4.9	0.25	0.57	5.82	2.70	0.26	0.59	5.95	2.83	4.00	3.51	2.23	4.81
2	187	29.7	23	4.6	0.08	0.78	6.23	2.88	0.09	0.81	6.26	2.98	4.65	3.85	0.48	3.47
3	170	30	24	4.8	0.33	0.43	4.72	2.33	0.32	0.42	4.85	2.4	3.03	2.33	2.75	3.00
4	177	30	20	4.5	0.19	0.51	6.64	2.98	0.18	0.53	6.78	3.12	4.76	3.92	2.11	4.70
5	182	29.5	22	4.8	0.14	0.70	6.10	2.89	0.13	0.72	6.37	3.0	4.41	2.86	4.43	3.81
6	175	30	24	4.9	0.26	0.54	5.27	2.38	0.25	0.56	5.39	2.42	3.85	3.70	2.28	1.68

curvature as a result of relationship between responses and independent variables; center points on the other hand are used to estimate the pure error. A complete design matrix with observed responses is shown in Table 3.

4 Results and discussion

4.1 Development of mathematical models

For the analysis of measured responses (FBH, BBH, FBW, and BBW) and development of best-fit mathematical models, commercial statistical software has been used. The adequacy of models, on the other hand, was tested using analysis of variance (ANOVA) technique.

4.1.1 Front bead height

The fit summary for FBH suggested quadratic relationship as the best-fit model. The ANOVA results revealed that main effects current (A), speed (C), gas flow rate (D), interaction effects current and voltage (AB), speed and gas flow rate (CD), and quadratic effect of current (A^2) were the significant model terms associated with FBH. The other model terms were insignificant and therefore eliminated by backward elimination to improve model adequacy. The reduced ANOVA table comprising of significant terms along with adequacy measure R^2, adjusted R^2, and predicted R^2 has been presented in Table 4. The results indicated that the model is significant (P value is less than 0.05). The adequacy measure R^2, adjusted R^2, and predicted R^2 are close to 1, indicating the adequacy of the resulting model. The final mathematical model for the FBH which can be successfully applied for the prediction is given in relation 5.

$$\text{Front Bead Height} = +1.03965 - (0.029671 \times \text{Current}) + (0.43167 \times \text{Voltage}) - (0.16953 \times \text{Speed}) - (0.77028\ \text{Gas flow rate}) - (0.00241667 \times \text{Current} \times \text{Voltage}) + (0.037000 \times \text{Speed} \times \text{Gas flow rate}) + (0.000249383 \times \text{Current}^2) \quad (5)$$

Fig. 5 Tensile test samples

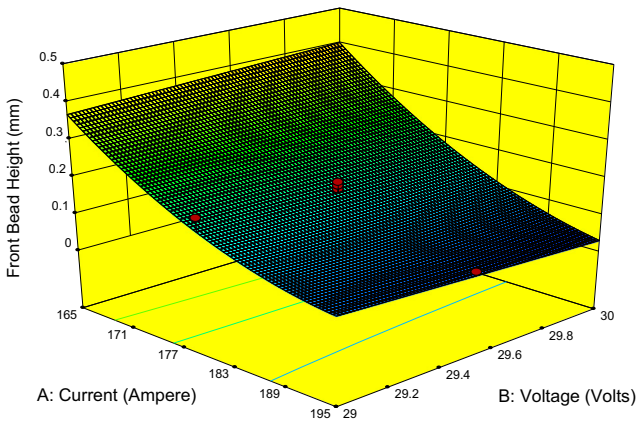

Fig. 6 3D response surface graph showing the effect of current and voltage on front bead height

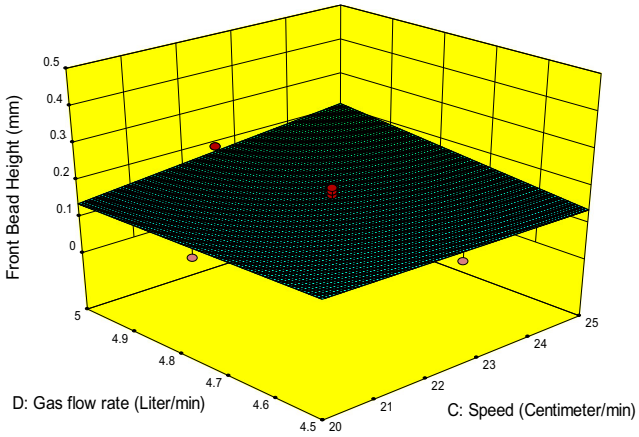

Fig. 7 3D response surface graph showing the effect of speed and gas flow rate on front bead height

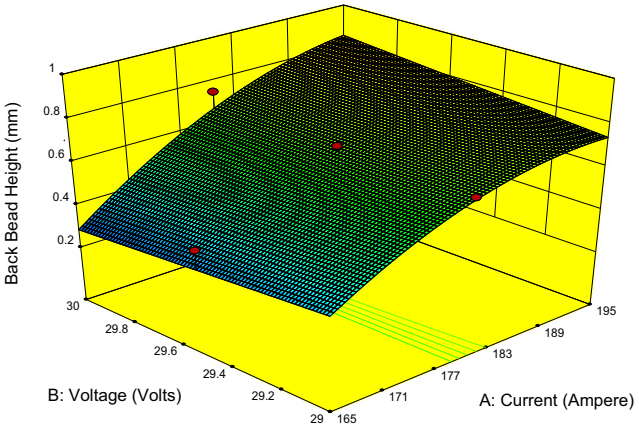

Fig. 8 3D response surface graph showing the effect of current and voltage on back bead height

4.1.2 Back bead height

The fit summary for BBH also highlighted the quadratic relationship as the best-fit relationship. The main interaction and quadratic factors that contribute significantly to BBH formation include current (A), current and voltage (AB), current and speed (AC), current and gas flow rate (AD), voltage and speed (BC), speed and gas flow rate (CD), and current (A^2). The reduced ANOVA results presented in Table 4 indicate that the model is significant (*P* value is less than 0.05). The developed mathematical model for the prediction of BBH is presented in Eq. 6.

$$\begin{aligned}\text{Back Bead Height} = {} & -14.0732 + (0.0143194 \times \text{Current}) \\ & - (0.726528 \times \text{Voltage}) + (1.04261 \times \text{Speed})(4.49472 \times \text{Gas flow rate}) \\ & + (0.0069167 \times \text{Current} \times \text{Voltage}) + (0.0006833 \times \text{Current} \times \text{Speed}) \\ & -(0.0115 \times \text{Current} \times \text{Gas flow rate}) - (0.0225 \times \text{Voltage} \times \text{Speed}) \\ & -(0.105 \times \text{Speed} \times \text{Gas flow rate}) - (0.0004543 \times \text{Current}^2)\end{aligned} \quad (6)$$

4.1.3 Front bead width

The quadratic relationship was found as the best-fit model for FBW. The main effects current (A), speed (C), interaction effects current and speed (AC), quadratic effects current (A^2), and gas flow rate (D^2) were identified as significant model terms associated with BBH. The ANOVA results of BBH after the elimination of insignificant terms are available in Table 4. With *P* value less than 0.05, the model is significant. The final mathematical model for the FBH which can be successfully applied for the prediction is given in Eq. 7.

$$\begin{aligned}\text{Front Bead Width} = {} & 97.0422 + (0.6218 \times \text{Current}) - (0.6651 \times \text{Speed}) \\ & -(59.8112 \times \text{Gas flow rate}) + (0.00245 \times \text{Current} \times \text{Speed}) \\ & -(0.00172 \times \text{Current}^2) + (6.28465 \times \text{Gas flow rate}^2)\end{aligned} \quad (7)$$

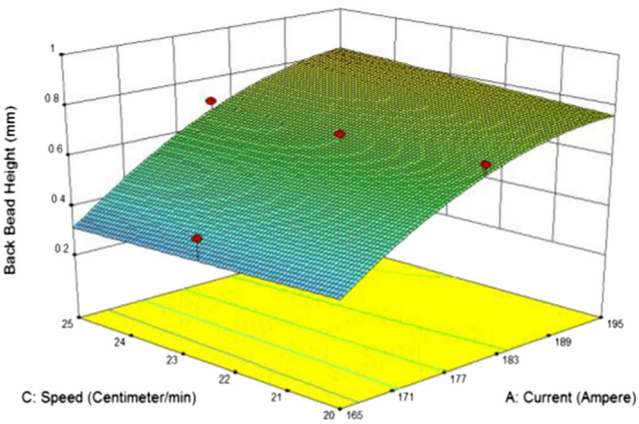

Fig. 9 3D response surface graph showing the effect of current and speed on back bead height

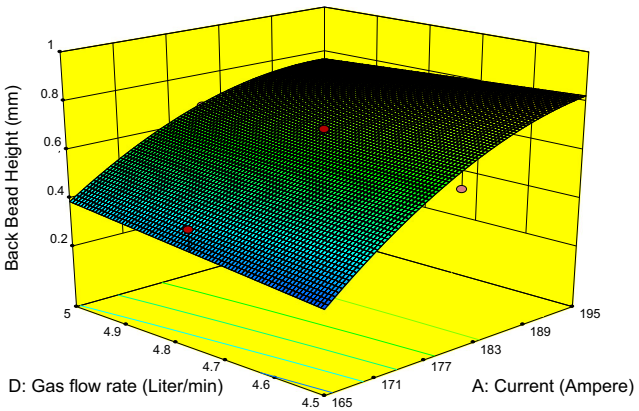

Fig. 10 3D response surface graph showing the effect of current and gas flow rate on back bead height

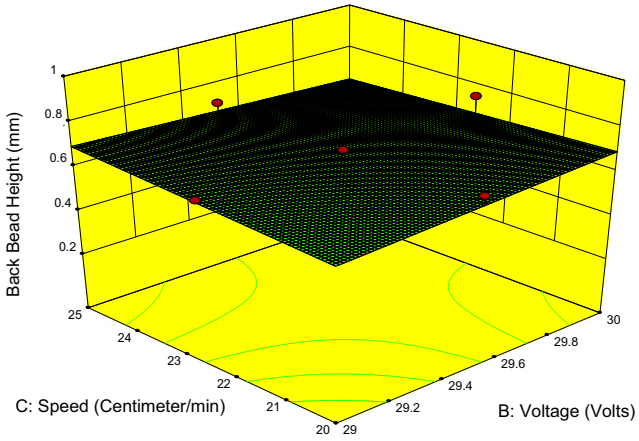

Fig. 11 3D response surface graph showing the effect of voltage and speed on back bead height

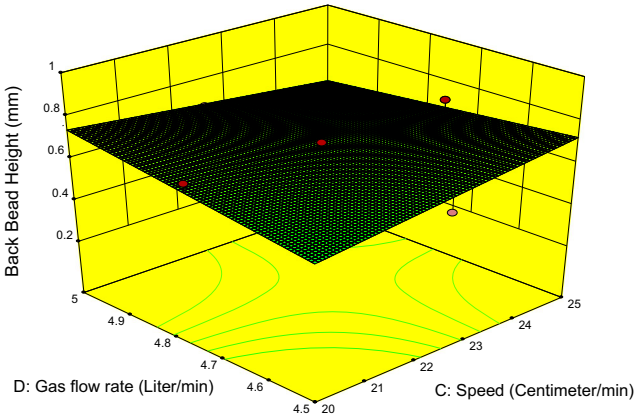

Fig. 12 3D response surface graph showing the effect of speed and gas flow rate on back bead height

4.1.4 Back bead width

The fit summary for FBW suggested a quadratic relationship as the best-fit model. The ANOVA results suggested that main effects current (A), speed (C), interaction effects current and speed (AC), speed and gas flow rate (CD), and quadratic effect current (A^2) are the significant model terms associated with BBH. The other model terms were insignificant and therefore eliminated by backward elimination to improve model adequacy. The reduced ANOVA table comprising of significant terms along with adequacy measure R^2, adjusted R^2, and predicted R^2 has been presented in Table 4. The results indicated that the model is significant (P value is less than 0.05). The adequacy measure R^2, adjusted R^2, and predicted R^2 are close to 1, indicating the adequacy of the resulting model. The final mathematical model for the FBH which can be successfully applied for the prediction is given in Eq. 8.

$$\begin{aligned}\text{Back Bead Width} = {} & 45.1189 - (0.48416 \times \text{Current}) + (0.4719 \times \text{Speed}) \\ & - (2.6697 \times \text{Gas flow rate}) - (0.00688 \times \text{Current} \times \text{Speed}) \\ & + (0.13080 \times \text{Speed} \times \text{Gas flow rate}) + \left(0.00187 \times \text{Current}^2\right)\end{aligned} \tag{8}$$

4.2 Adequacy measure and validation of the developed models

The developed models have been verified for their adequacy through statistical analysis. In addition, confirmation experiments were performed to validate the models experimentally. The predicted versus actual responses of FBH, BBH, FBW, and BBW are shown in Fig. 4a–d, respectively. It is evident from the figures that predicted and actual points lie on or close to the straight line indicating that errors are normally distributed. Thus, it can be claimed that the proposed models are adequate and there is no chance of any violation of independence or constant variation assumption.

To validate the developed model experimentally, six confirmation experiments were conducted with randomly chosen

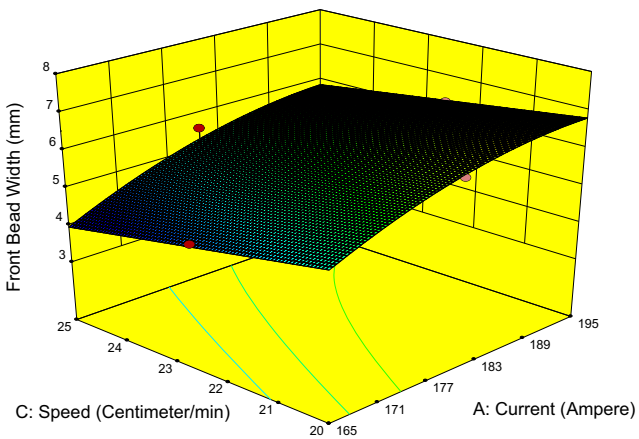

Fig. 13 3D response surface graph showing the effect of current and speed on front bead width

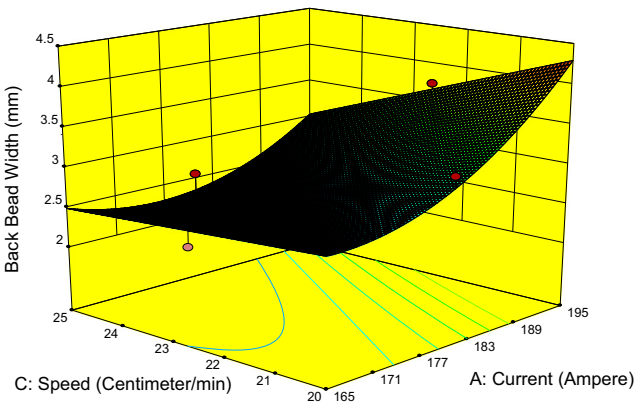

Fig. 14 3D response surface graph showing the effect of current and speed on back bead width

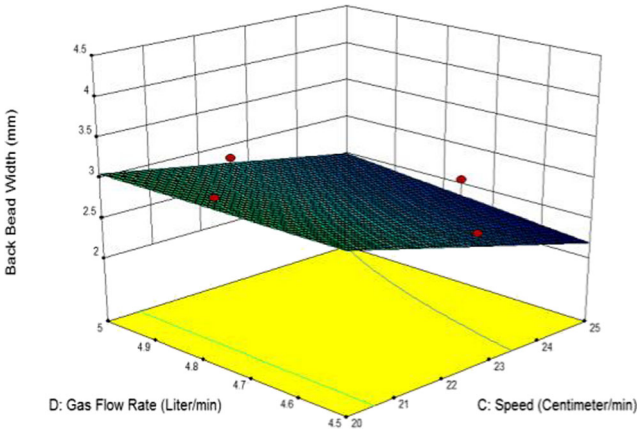

Fig. 15 3D response surface graph showing the effect of speed and gas flow rate on back bead width

welding conditions (different from CCD used for the development of models) within design space. The results of confirmation experiments are presented in Table 5. To clearly visualize the difference between predicted and actual values, the percentage error was calculated through relation 9 and has been provided in Table 5. Results show that percentage error is less than 5 %, which validates the empirical models developed for the prediction. Furthermore, it can be established from the results that the developed models have the capability to predict the responses accurately with minor deviation.

$$\text{Percentage error} = \left|\frac{\text{actual value}-\text{predicted value}}{\text{predicted value}}\right| \times 100 \quad (9)$$

Table 6 Summary of main and interaction factors affecting the weld bead geometry

	Front bead height (mm)	Back bead height (mm)	Front bead width (mm)	Back bead width (mm)
Current: A	✓	✓	✓	✓
Voltage: B				
Speed: C	✓		✓	✓
Gas flow rate: D	✓			
Current × voltage: A × B	✓	✓		
Current × speed: A × C		✓	✓	✓
Current × gas flow rate: A × D		✓		
Voltage × speed: B × C		✓		
Voltage × gas flow rate: B × D				
Speed × gas flow rate: C × D	✓	✓		✓

To verify the strength of the welded joints, tensile strength tests were also carried out. Six samples were randomly chosen from 30 experiments performed for the model development. Tensile samples were made as per ASME section IX, boiler, and pressure vessel code. The Universal Testing Machine EDC (250 KN/25 Ton) was used for tensile testing. The tensile-tested samples are shown in Fig. 5. It is evident from the figure that the failure in all samples occurred at the section away from the welded region.

4.3 3D response surface

The response surface plots shown in Figs. 5, 6, 7, 8, 9, 10, 11, 12, 13, and 14 demonstrate the effects of significant welding parameters on weld bead geometry. The objective is to minimize all response variables. Figures 6, 7, 8, 9, 10, 11, 12, 13, 14, and 15 show the effects of two significant welding parameters (simultaneously) on response variables (FBH, BBH, FBW, and BBW) at the middle levels of other welding parameters. Figure 6 shows the effect of current and voltage on FBH. It is evident from Fig. 6 that FBH is more influenced by current than voltage. Furthermore, the FBH is minimum at high current and low voltage, and maximum at low current and high voltage. Figure 7 demonstrates the effects of speed and gas flow rate on FBH. It can be seen that minimum FBH is achieved at lowest levels of speed and gas flow rate. Figure 8 reflects the effects of current and voltage on BBH. It is observed that BBH is affected more by current as compared to voltage. It is also worth noting that minimum BBH can be obtained at lowest level of current and voltage. Figure 9 presents the effects of current and speed on BBH. The results indicate that BBH is highly affected by current as compared to speed. The effects of current and gas flow rate on BBH have been provided in Fig. 10. It is evident from the figure that current has more effect on BBH as compared to gas flow rate. Furthermore, at low levels of current, BBH decreases by decreasing gas flow rate, whereas at high levels of current, BBH increases by increasing gas flow rate. Figure 11 represents the effects of voltage and speed on BBH. Minimum BBH is achieved at the highest level of voltage and speed. However, it is noteworthy that the value of BBH remains constant, i.e., 0.65 mm at the highest level of voltage and lowest level of speed, or lowest level of voltage and highest level of speed. The 3D relationship of speed and gas flow rate with BBH (Fig. 12) is similar to that of voltage and speed relationship with BBH (Fig. 11).

The effects of current and speed on FBW and BBW are shown in Figs. 13 and 14, respectively. It is observed that minimum FBW is obtained at the lowest level of current and highest level of speed. The lowest current and speed have minor effect on BBH. The effect of speed is

considerably very large at high levels of current. However, the effect of current remains almost the same at all levels of speed. It is noteworthy that minimum BBH is obtained at center level of current (Fig. 14). Finally, Fig. 15 describes the effects of variation in speed and gas flow rate on BBW. It is clear from the figure that BBW decreases with the increase in speed. The effect of gas flow rate is negligibly small at low speed and vice versa.

The above discussion represents the interaction effects of performance measures individually. However, FBH, BBH, FBW, and BBW contribute equally to achieve high weld quality. Therefore, the input parameters (current, voltage, speed, and gas flow rate) need to be controlled in such a way that optimum results could be achieved. Table 6 represents the summary of main and interaction factors affecting the weld bead geometry. It is clear from Table 6 that current is the main contributing factor which controls all sub-factors of weld bead geometry. Speed is the second factor which influences all sub-factors of weld bead geometry except BBH. Gas flow rate, on the other hand, influences the FBH only. The interaction factor current × voltage influences FBH and BBH, whereas, current × speed affects all sub-factors of weld bead geometry except FBH. Similarly, speed × gas flow rate significantly influences all sub-factors of weld bead geometry except FBW. In addition to these factors, BBH is also influenced by interaction of current × gas flow rate and voltage × speed.

5 Conclusions

The aim of the research was to develop empirical models for the prediction of weld bead geometry of HSLA steel using PAW process. The effects of different welding parameters, i.e., current, voltage, welding speed, and plasma gas flow rate, were quantified using face-centered CCD.

The experimental results demonstrate that current is the most significant factor affecting all four responses, i.e., front bead height, back bead height, front bead width, and back bead width. Higher value of current with low welding speed results in larger front bead width. Therefore, lower current with higher welding speed is recommended for optimum front bead width. To achieve more penetration, values of current should be kept high and vice versa. Furthermore, values of back bead width will be more at lower welding speed and higher current.

The confirmation experiments were found in close approximation to empirical models with percentage error less than 5 %. The validation results confirmed the capability of empirical models to predict the responses accurately. In the future, these models will be helpful for practitioners to determine input parameters setting for optimum weld bead geometry.

References

1. Xu WH, Lin SB, Fan CL, Yang CL (2014) Evaluation on microstructure and mechanical properties of high-strength low-alloy steel joints with oscillating arc narrow gap GMA welding. Int J Adv Manuf Technol 75(9–12):1439–1446
2. Connor LP, O'Brien RL (1991) Welding handbook: welding processes (Vol. 2). American Welding Society, USA
3. Wu CS, Wang L, Ren WJ, Zhang XY (2014) Plasma arc welding: process, sensing, control and modeling. J Manufac Process 16(1): 74–85
4. Keanini RG, Rubinsky B (1990) Plasma-arc welding under normal and zero gravity. Weld J 69(6):41–50
5. Teker T, Özdemir N (2012) Weldability and joining characteristics of AISI 430/AISI 1040 steels using keyhole plasma arc welding. Int J Adv Manuf Technol 63(1–4):117–128
6. Feng Y, Luo Z, Liu Z, Li Y, Luo Y, Huang Y (2015) Keyhole gas tungsten arc welding of AISI 316L stainless steel. Mater Des 85: 24–31
7. Migiakis K, Daniolos N, Papadimitriou GD (2010) Plasma keyhole welding of UNS S32760 super duplex stainless steel: microstructure and mechanical properties. Mater Manuf Process 25(7):598–605
8. Prasad KS, Rao CS, Rao DN (2012) Study on factors effecting weld pool geometry of pulsed current micro plasma arc welded AISI 304L austenitic stainless steel sheets using statistical approach. J Miner Mater Charact Eng 11:790–799
9. Prasad KS, Rao CS, Rao DN (2011) Prediction of weld pool geometry in pulsed current micro plasma arc welding of SS304L stainless steel sheets. Int Trans J Eng Manag Appl Sci Technol 2(3):325–336
10. Juang S, Tarng Y (2002) Process parameter selection for optimizing the weld pool geometry in the tungsten inert gas welding of stainless steel. J Mater Process Technol 122:33–37
11. Iqbal A, Khan SM, Mukhtar HS, (2011) ANN assisted prediction of weld bead geometry in gas tungsten arc welding of HSLA steels. In Proceedings of the World Congress on Engineering WCE 2011, July 6–8, 2011, London, UK
12. Prasad KS, Chalamalasetti SR, Damera NR (2015) Application of grey relational analysis for optimizing weld bead geometry parameters of pulsed current micro plasma arc welded Inconel 625 sheets. Int J Adv Manuf Technol 78(1–4):625–632
13. Prasad KS, Ch SR, Rao N (2010) Prediction of weld quality in plasma arc welding using statistical approach. AIJSTPME 3(4): 29–35
14. Al-Faruk A, Hasib A, Ahmed N, Das UK (2010) Prediction of weld bead geometry and penetration in electric arc welding using artificial neural networks. Int J Mech Mechatronics Eng 10:19–24
15. Kumar V (2011) Modeling of weld bead geometry and shape relationships in submerged arc welding using developed fluxes. Jordan J Mech Ind Eng 5(5):461–470
16. Lalitnarayan K, Sarcar MMM, Rao KM, Kameswaran K (2011) Prediction of weld bead geometry for CO_2 welding process by multiple regression analysis. Int J Math Sci Comput 1(1):52–57
17. Liu Z, Wu CS, Gao J (2013) Vision-based observation of keyhole geometry in plasma arc welding. Int J Therm Sci 63:38–45
18. Siva K, Murugan N, Logesh R (2009) Optimization of weld bead geometry in plasma transferred arc hardfaced austenitic stainless steel plates using genetic algorithm. Int J Adv Manuf Technol 41(1–2):24–30
19. Zhang G, Wu CS, Liu X (2015) Single vision system for simultaneous observation of keyhole and weld pool in plasma arc welding. J Mater Process Technol 215:71–78
20. Murugan N, Gunaraj V (2005) Prediction and control of weld bead geometry and shape relationships in submerged arc welding of pipes. J Mater Process Technol 168:478–487

21. Wu CS, Jia CB, Chen MA (2010) A control system for keyhole plasma arc welding of stainless steel plates with medium thickness. Weld J 89(11):225–231
22. Narang H, Singh U, Mahapatra M, Jha P (2011) Prediction of the weld pool geometry of TIG arc welding by using fuzzy logic controller. Int J Eng Sci Technol 3:77–85
23. Shoeb M, Parvez M, Kumari P (2013) Effect of MIG welding input process parameters on weld bead geometry on HSLA steel. Int J Eng Sci Technol 5:200–212
24. Benyounis K, Olabi A, Hashmi M (2005) Effect of laser welding parameters on the heat input and weld-bead profile. J Mater Process Technol 164:978–985
25. Goyal V, Ghosh P, Saini J (2009) Analytical studies on thermal behaviour and geometry of weld pool in pulsed current gas metal arc welding. J Mater Process Technol 209:1318–1336
26. Zhang GJ, Yan ZH, Lin WU (2006) Visual sensing of weld pool in variable polarity TIG welding of aluminium alloy. Trans Nonferrous Metals Soc China 16(3):522–526
27. Azam M, Jahanzaib M, Wasim A, Hussain S (2015) Surface roughness modeling using RSM for HSLA steel by coated carbide tools. Int J Adv Manuf Technol 78(5–8):1031–1041
28. Montgomery DC (2001) Design and analysis of experiments 5th edition. John Wiley and Sons, New York